



A new magnetorheological quasi-zero stiffness vibration isolation system with large zero stiffness range and highly stable characteristics

Lei Deng · Shuaishuai Sun · Qihao Wu · Ning Gong · Jiang Yang ·
Shiwu Zhang · Haiping Du · Weihua Li

Received: 28 March 2023 / Accepted: 19 August 2023 / Published online: 6 September 2023
© The Author(s) 2023

Abstract Various quasi-zero stiffness (QZS) systems have been developed and applied in the vibration control domain in recent years. However, most QZS systems are usually unstable against external disturbances, and their QZS ranges are very limited. To address these issues, this study develops a highly stable QZS vibration isolation system integrated with magnetorheological fluids (MRFs). The MRFs endow the vibration isolation system with stiffness variability in vertical and lateral directions to against external

disturbances, which innovatively solves the unstable problem of QZS systems. Meanwhile, the stiffness variability also makes the system adaptable to vibrations with different frequencies, so the system can deliver the best vibration isolation performance in response to various excitations. The system consists of a vertical isolation unit and a lateral isolation unit. By paralleling a nonlinear positive stiffness QZS component with a nonlinear negative stiffness QZS component in the vertical isolation unit, a large QZS range in the vertical direction and smaller stiffness are realised, thus improving the vibration isolation performance. In this study, the vibration isolation system is designed

Supplementary Information The online version contains supplementary material available at <https://doi.org/10.1007/s11071-023-08856-2>.

L. Deng (✉) · H. Du
School of Electrical, Computer and Telecommunications Engineering, University of Wollongong, Wollongong, NSW 2522, Australia
e-mail: leideng@uow.edu.au

S. Sun (✉) · N. Gong · S. Zhang
CAS Key Laboratory of Mechanical Behavior and Design of Materials, Department of Precision Machinery and Precision Instrumentation, University of Science and Technology of China, Hefei 230027, Anhui, China
e-mail: sssun@ustc.edu.cn

Q. Wu
Department of Industrial and Manufacturing Systems Engineering, The University of Hong Kong, Pok Fu Lam, Hong Kong, China

J. Yang
School of Electrical Engineering and Automation, Anhui University, Hefei 230039, Anhui Province, China

W. Li
School of Mechanical, Materials, Mechatronic and Biomedical Engineering, University of Wollongong, Wollongong, NSW, Australia

and prototyped; its QZS characteristics and adjustable stiffness features in both the vertical and lateral directions are experimentally verified; the frequency responses of the system are obtained experimentally; and the stability and the vibration isolation performance of the system are also evaluated by experiments with the designed control algorithms. This study provides a solution to overcome the unstable problem of QZS systems and extend the limited QZS range, whilst realising QZS characteristics in both vertical and lateral directions, thus broadening the application of QZS systems.

Keywords Quasi-zero stiffness · Vibration isolation · Magnetorheological fluids · Tunable stiffness · Stability

1 Introduction

Vibration is a common phenomenon in nature and the daily life of human beings. A large majority of vibration is undesirable, such as the vibration of vehicles caused by road unevenness, the vibration of buildings induced by earthquakes and strong winds, and the vibration of aeroplanes when they suffer turbulent air. The undesirable vibration of a machine may cause mechanical failure, shorten its lifespan and increase maintenance costs. It can also be a severe threat to people's health and safety. For instance, long-term suffering of drivers from vibration could induce diseases such as lumbago, backache and lower back pain [1, 2]. To reduce the influence of the undesirable vibration, various methods have been developed, such as vibration reduction by using advanced devices and control algorithms [3–8], vibration absorption by attaching absorbers to the vibration body [9–11] and vibration isolation by installing isolators between the vibration source and the protected structure [12–16].

Vibration isolation is a method to isolate the protected objective from the source of vibration, such as a vibration isolator that hinders the vibration transferred from the land to the building during an earthquake [17–21]. As one of the vibration isolation devices, the quasi-zero stiffness (QZS) isolation system has received much research attention [22–29]. The pioneer book of Alabuzhev et al. [30] systematically introduced the vibration protecting

system featuring QZS characteristics. QZS mechanisms are usually achieved by combining negative stiffness elements with positive stiffness elements. A simple QZS system is the three-spring structure which comprises one vertical linear spring and two nonlinear prestressed oblique springs. Carrella et al. [31] investigated the static characteristic of a quasi-zero stiffness isolator consisting of three springs, and Kovacic et al. [32] further analysed its dynamic characteristic. To make the three-spring structure more compact, Lan et al. [33] replaced the coil springs with planar springs. Lateral and vertical adjustment mechanisms were also designed to make the QZS achievable under imperfect conditions and enable the isolator to apply to different loads. Zhao et al. [34] refined the three-spring structure by using two pairs of oblique springs instead of one pair to increase the quasi-zero stiffness region, thus improving the isolation performance. Other QZS structures [35–46] have also been developed, for instance, Zhou et al. [47] proposed a QZS system based on the mechanism of cam–roller–spring; Liu et al. [48] reported a structure that parallels a linear spring with the Euler buckled beams; and Shaw et al. [49] presented a design consisting of linear springs in parallel with the transverse flexure of a composite bistable plate.

Even though a large number of designs have been reported, QZS systems still have disadvantages that should be overcome to broaden their application. One disadvantage is that most QZS systems are inherently unstable to external disturbances. The stiffness of QZS systems is usually very low, so even a small external disturbance can induce a large displacement and make it dysfunctional. Another disadvantage is that the QZS range, in which the stiffness is close to zero, is usually limited. This QZS range is the most effective range for vibration isolation. Hence, the isolation performance can be improved by expanding the QZS range. To address the unstable problem, this paper designs a highly stable QZS vibration isolation system by integrating magnetorheological fluids (MRFs). MRFs are a kind of smart material whose rheological property can be changed by regulating the applied magnetic field [50–52]. The integrated MRFs can make the stiffness of the system tunable, so large stiffness can be applied once the system suffers external disturbances, making the system highly stable. The stiffness variability also makes the system adaptable to various vibrations with different

frequencies, hence realising the best vibration isolation performance in response to various excitations. The proposed system consists of vertical and lateral isolation units that can isolate the vertical and lateral vibrations, respectively. In the vertical isolation unit, a nonlinear positive QZS component is paralleled with a nonlinear negative QZS component, so a much wider QZS range than the conventional QZS systems with smaller stiffness can be realised, which overcomes the disadvantage of the limited QZS range and improves the vibration isolation performance. The innovation and novelty of this paper are summarised as follows:

- (1) A novel quasi-zero stiffness vibration isolation system integrated with magnetorheological fluids capable of simultaneously isolating the vertical and lateral vibrations was designed and prototyped.
- (2) The stiffness variability endowed by the magnetorheological fluids significantly increases the stability of the isolation system when it suffers external disturbances whilst improving the vibration isolation performance as the stiffness variability makes the system adaptable to various vibrations.
- (3) In the vertical isolation unit of the system, a nonlinear positive QZS component is paralleled with a negative QZS component, which expands the quasi-zero stiffness range for isolating vibrations.

The rest of this paper is organised as follows. The structural design and mathematical modelling of the proposed QZS vibration isolation system are detailed in Sect. 2. Section 3 presents the characterisation of the quasi-zero stiffness and tunable stiffness characteristics. In Sect. 4, the frequency response tests of the vertical and lateral isolation units are introduced. Then, the stability and vibration isolation performances of the system are experimentally evaluated in Sect. 5. Finally, the conclusion is drawn in Sect. 6.

2 Structural design, working principle and mathematical modelling

2.1 Structural design and working principle

As shown in the schematic diagram (Fig. 1a), the proposed vibration isolation system consists of a

vertical isolation unit (#1), a lateral isolation unit (#2) and a wooden support frame (#3) that connects them. Each unit integrates the QZS characteristic and the tunable stiffness feature to achieve a stable QZS characteristic. With these two units, the proposed isolation system can attenuate the vibrations transmitted from the base to the preloaded mass (the protected target) in both the vertical and lateral directions via the QZS characteristic; meanwhile, the stability of the system is improved by the tunable stiffness characteristic to against the external disturbances acted on the preloaded mass, and the vibration isolation performance is also improved because the stiffness can adapt to vibrations with different frequencies. The photograph of the prototyped isolation system is presented in Fig. 1b. The specific designs and the working principles of the vertical and lateral isolation units are detailed in the following two subsections.

2.1.1 The vertical isolation unit

As shown in Fig. 2a, the vertical isolation unit mainly comprises a preloaded mass (#1), top and base plates (#2 and 6), three linear rod-bearing structures (#3), a geometric anti-spring (GAS) structure (#4), three magnetic negative stiffness (MNS) dampers (#5 and Fig. 2b) and a variable stiffness (VS) structure (Fig. 2c). Guided by the linear rod-bearing structures, the top and base plates move vertically. The QZS characteristic of the vertical isolation unit is realised by paralleling the nonlinear positive stiffness QZS component (the GAS structure) with the nonlinear negative stiffness QZS components (three MNS dampers). The GAS structure and the MNS dampers possess different force–displacement patterns featuring positive and negative stiffness and with a QZS range in the middle section of their strokes. By superpositioning their force–displacement patterns, a wider QZS range than each of them is achieved. Meanwhile, the VS structure makes the QZS characteristic more stable by adding the variable stiffness feature, so the vertical unit can also resist external disturbances. Besides, the stiffness variability also endows the isolation unit with ability to isolate different vibration excitations with various frequencies.

The GAS structure consists of a preloaded mass (#1), a central plate (#8), six blad springs (#9) and six clamps (#10). The clamps are angularly mounted on

Fig. 1 Vibration isolation system. **a** Sectional view. **b** Photograph

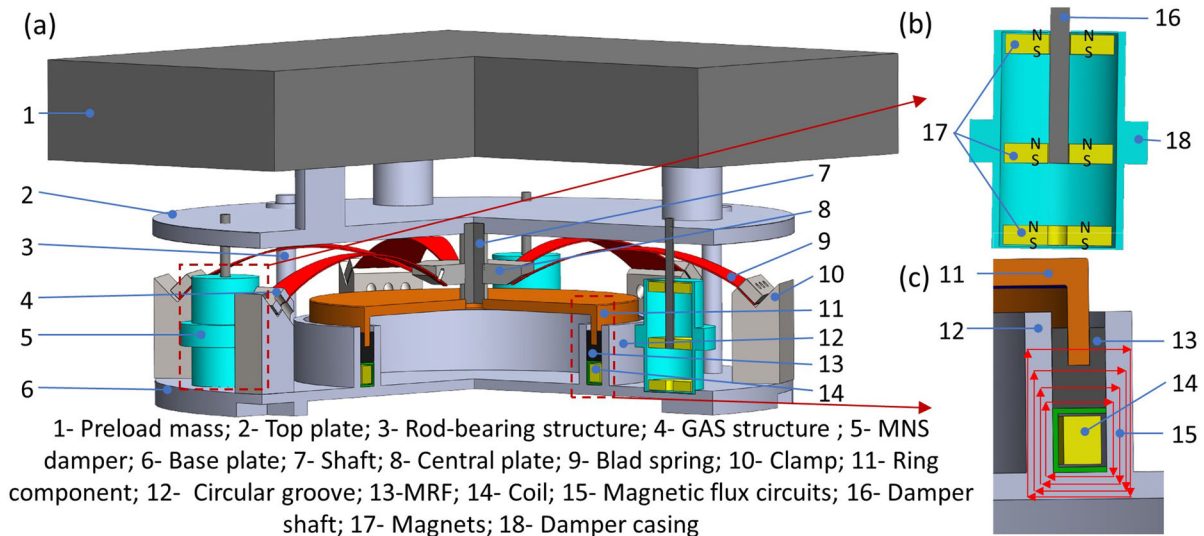
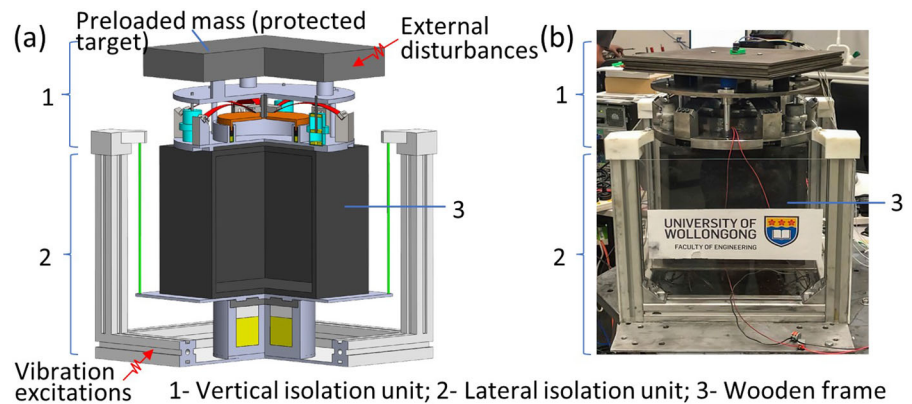


Fig. 2 Vertical isolation unit. **a** Sectional view; **b** MNS damper; **c** VS structure

the base plate, and adjacent clamps form an angle of 60° . Each blad spring is fixed to one clamp on one end and the central plate on the other. The central plate is connected to the top plate and the preload, so blad springs are precompressed. By adjusting the preloaded mass, the initial position of the vertical isolation unit is in the middle position of the QZS range, which optimises the vibration isolation performance.

As shown in Fig. 2b, an MNS damper comprises a damper shaft (#16), three ring magnets (#17, material: Nd2Fe14B) and a 3D printed damper casing (#18). The middle magnet is fixed to the damper shaft, and the other two are fixed to the casing on the top and bottom. The damper shaft and the casing are fastened to the top and the base plates of the vertical isolation unit, respectively. When the relative motion of the top

and base plates is induced by vibration, the middle magnet will move relative to the upper and lower magnets. At the initial state, the middle magnet is positioned at the middle stroke, and the attractive forces acted by the upper and lower magnets are balanced. It is known that the attractive forces between the magnets with the same pole arrangement increase with the decrease in their distance. Hence, if the middle magnet moves up, the attractive force of the top magnet will be larger than that of the lower one; therefore, the resultant force is in the same direction of the motion, and the damper behaves with a negative stiffness characteristic.

The VS structure is detailed in Fig. 2c. A circular coil (#14) covered by a 3D printed frame is fastened in a circular groove (#12) of the base plate, in which

MRFs (#13, MRF-122EG, Lord Corp.) are filled. A ring component (#11), which is fixed to the shaft and the central plate, is partially immersed in the MRFs. If a current is applied to the coil, magnetic flux circuits (#15) shown in Fig. 2c will be generated immediately. At the same time, the MRFs will rapidly transform from the free-flowing liquid state to the semisolid state, and its viscosity will dramatically increase, which significantly hinders the movement of the ring component and increases the stiffness of the system. Because the viscosity of MRFs can be regulated by the current, the stiffness of the vertical isolation unit can be controlled by regulating the current accordingly.

2.1.2 The lateral isolation unit

Figure 3 shows the lateral isolation unit for isolating the vibration in the horizontal direction. In order to achieve an ideal isolation effect, especially in low-frequency vibration isolation conditions, the pendulum structure, which can isolate horizontal vibrations and is featured with a QZS characteristic, was selected in this design. Additionally, MRFs are also utilised in the isolation unit to vary the stiffness. The sectional view of the unit is provided in Fig. 3a. It is seen that an isolated plate (#3) is hung to the four corners of an aluminum extrusion frame (#1) with wires (#2), forming a pendulum structure. Meanwhile, the circular bulge (#6) and the ring bulge (#7) of the isolated plate are immersed in the MRFs (#4, MRF-122EG, Lord Crop.), which are filled in the groove of an electromagnet (#5). The electromagnet is fixed to the

base of the extrusion frame, and the gap between the electromagnet and the hung plate is controlled as 1 mm by adjusting the length of the wires. As demonstrated in Fig. 3b, a coil (#8) is seated in the electromagnet, and an aluminium component (#9) is also installed to optimise the magnetic flux path. Without a current applied to the coil, the plate can move almost freely in the lateral direction because the viscosity at this state is very low. In contrast, when a current is applied to the electromagnet, magnetic flux circuits (#10) shown in Fig. 3b will be induced. At the same time, the viscosity of the MRFs increases drastically, so the relative motion between the isolated plate and the electromagnet is restrained, and the lateral stiffness of the lateral isolation unit is increased consequently. As the viscosity of MRFs can be controlled by regulating the magnitude of the current, the lateral stiffness of the isolation unit can also be controlled accordingly.

2.2 Mathematical modelling of the vertical isolation unit

As the matching of the GAS structure and the MNS dampers is crucial for the vertical isolation unit to acquire a large QZS range, this section will mainly focus on the modelling of the GAS structure, the MNS dampers and their superposition to realise a QZS characteristic with a large QZS range.

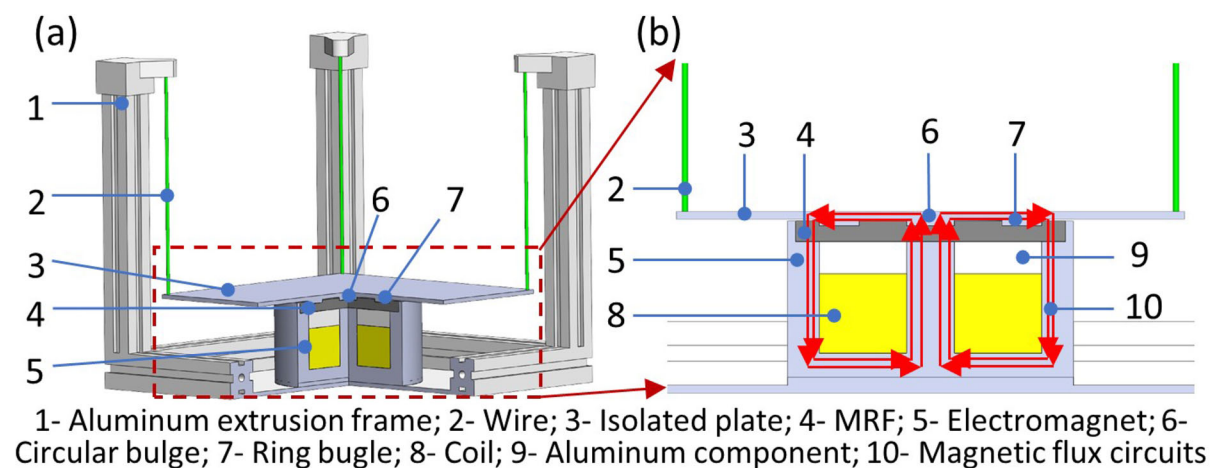


Fig. 3 Lateral isolation unit. **a** Sectional view; **b** Local view

2.2.1 Modelling of the GAS structure

The GAS structure reported in Yan’s research [53, 54] was selected as the nonlinear positive stiffness component. The blade spring of the GAS structure is presented in Fig. 4a. According to the research [53, 54], the shape function of the blade spring is expressed as:

$$\gamma(\xi) = \frac{\omega(l)}{\omega(0)} = [c_1 + c_2 \cos(\beta\xi) + c_3 \sin(\beta\xi)]^{-1} \quad (1)$$

where $\xi = l/L$, $\omega(0) = 36 \text{ mm}$, $c_1 = -0.377$, $c_2 = 1.377$, $c_3 = 0.195$, and $\beta = 1.361$.

As the GAS structure is centrosymmetric with all the force acting on six blade springs via the central plate, the mechanical property of the GAS structure can be acquired by analysing one single blade spring, as shown in Fig. 4b. The origin O is located at the connection point of the blade spring and the clamp, X axis represents the direction towards the central plate in the horizontal direction, and Y axis represents the vertical direction. The point (X, Y) is at the connection point of the blade spring and central plate. F_X and F_Y are the horizontal constraint force and the vertical force, respectively. The dimensionless force of the point (X, Y) in the vertical direction, G_Y , is introduced, and it is expressed as:

$$G_Y = \frac{12L^2}{Ed^2w(0)} F_Y \quad (2)$$

where $E = 211 \text{ GPa}$ is the Young’s modulus of the material of the blade spring, $d = 0.78 \text{ mm}$ is the thickness, F_Y is the actual force of the point (X, Y) in vertical directions and $L = 120 \text{ mm}$ is the length of the blade spring.

According to the literature [54], the relationship between the dimensionless force G_Y and the dimensionless vertical displacement for different geometric parameters can be fitted by:

$$G_Y(y) = \sum_{i=1}^7 a_i y^i \quad (3)$$

where $y = y_L - y_L|_{G_Y=0}$, and $y_L = Y/L = \int_0^1 \sin \xi d\xi$ is the dimensionless vertical coordinate of the GAS structure. $a_i (i = 1, 2, 3, 4, 5, 6, 7)$ are the fitting coefficients, and their values are decided by referring Table 3 of the literature [54] for a predefined x_L . Under a full consideration to achieve a QZS characteristic with a wide range stroke, x_L is set as 0.91 in this research. Hence, with the confirmed a_i , Eq. (3) is expressed as:

$$G_Y(y) = 32.63y - 298.54y^2 + 1808.39y^3 - 7651.96y^4 + 21186.12y^5 - 32719.64y^6 + 21726.28y^7 \quad (4)$$

From the above equations, the relationship between the vertical force F_Y and the vertical displacement Y of the GAS structure can be acquired. The simulation result is compared with the experimental one in Fig. 5, where the experimental results were obtained by testing the prototyped GAS structure with an MTS testing system which will be presented in Sect. 3.1. It is observed from the figure that both the experimental and theoretical data indicate the GAS structure behaves with a positive stiffness feature: the force increases with the increase in the displacement. The experimental and theoretical data have a similar trend

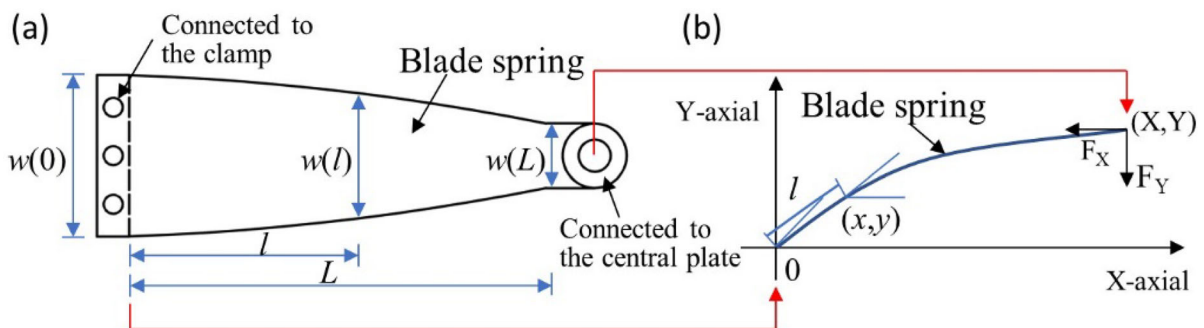


Fig. 4 Blade spring. a Shape; b Mechanical model

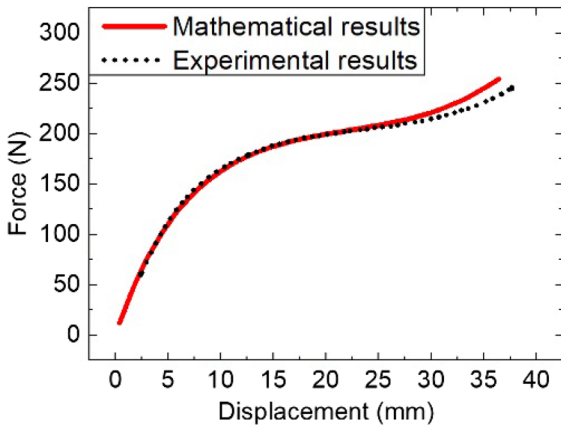


Fig. 5 Comparison of mathematical and experimental results of the GAS structure

of changing stiffness, which decreases from the large stiffness in the small displacement range to quasi-zero stiffness at the medium part, prior to the following growth of the stiffness in the large displacement range. It is also noticed that the mathematical and experimental results are matched very well, indicating good mathematical modelling is done.

2.2.2 Modelling of MNS dampers

Three MNS dampers are installed between the top and base plates of the vertical isolation unit to offer nonlinear negative stiffness characteristics. As detailed in Fig. 6, the top and bottom magnets of the MNS damper are fixed to the damper casing. The middle one is fixed to a shaft, so it can move up and down following the movement of the vertical vibration isolation unit. These ring magnets have the same configuration, and their magnetic poles are arranged in the same direction as well: the north pole is on the top

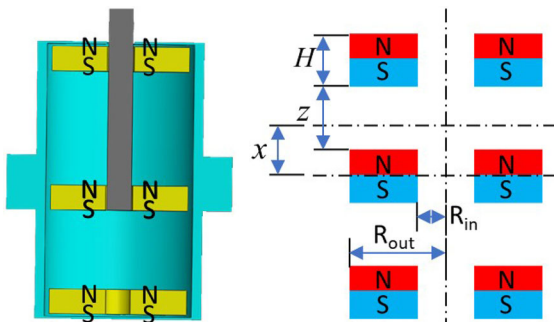


Fig. 6 Schematic of the MNS damper and its modelling

and the south pole is under the bottom. x in the figure is the transient displacement of the middle magnet; z is the distance between the top and middle magnets; $H = 5 \text{ mm}$, $R_{in} = 5.5 \text{ mm}$ and $R_{out} = 28 \text{ mm}$ are the thickness, inside radius and outside radius of the magnets, respectively.

Referencing the literature [55], the total force of three MNS dampers, F_N , can be calculated by:

$$\begin{aligned}
 F_N &= 3F_D \\
 F_D &= R_{out}, R_{in}, H, z, x \\
 &= \sum_{i=1}^8 \int_{\theta_1=0}^{2\pi} \int_{\theta_2=0}^{2\pi} \int_{r_1=R_{in}}^{R_{out}} \int_{r_2=R_{in}}^{R_{out}} y_i a(y_i) \times r_1 r_2 dr_1 dr_2 d\theta_1 d\theta_2 \\
 y_1 &= z - x; y_2 = z - x; y_3 = z - x - H; y_4 = z - x \\
 &+ H; y_5 = -z - x; y_6 = -z - x; y_7 = -z - x - H; y_8 = -z - x + H
 \end{aligned} \tag{5}$$

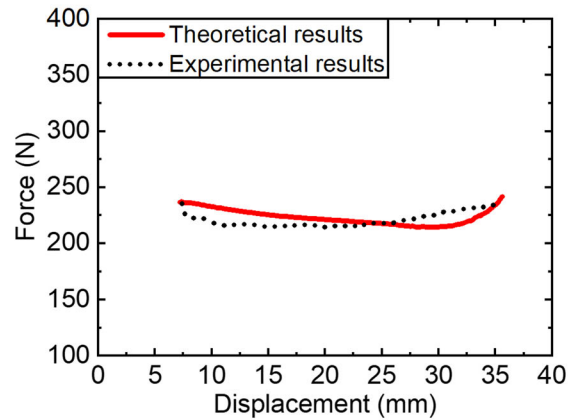
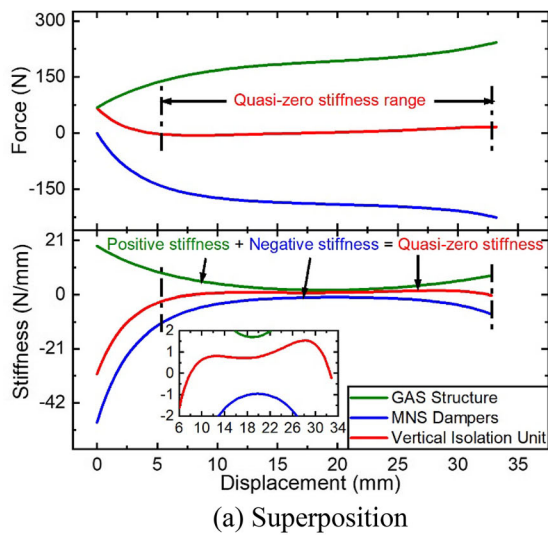
where F_D is the damper force of one MNS damper and $a(y_i)$ is expressed as:

$$a(y_i) = \frac{\sigma^2}{4\pi\mu_0} \cdot \frac{1}{(2r_{out}^2 - 2r_{out}^2 \cos(\theta) + y_i^2)^{\frac{3}{2}}} \tag{6}$$

where σ in the equation is the magnetic pole density of the magnets, and it is set as $\sigma = 1.28$ based on the material of $\text{Nd}_2\text{Fe}_{14}\text{B}$ [56]. $\mu_0 = 1.2567 \times 10^{-6} \text{ H/m}$ is the permeability of the vacuum.

2.2.3 Superposition of the GAS structure and MNS dampers

The concept of quasi-zero stiffness is realised by superpositioning the positive stiffness and negative stiffness, namely by paralleling the GAS structure with the MNS dampers. Based on the established mathematical modelling, the force–displacement responses of the GAS structure, MNS dampers and the vertical isolation unit are provided in Fig. 7a. It is seen that the GAS structure and the MNS dampers behave nonlinear positive and negative stiffness characteristics, respectively. In their middle displacement ranges, the stiffness is very low and close to zero. Here, the QZS characteristic is deemed as the stiffness smaller than $\pm 2 \text{ N/mm}$. As indicated by the figure, the QZS ranges for GAS structure and MNS dampers are 16–22 mm and 12.8–26.8 mm, respectively, both of which are very limited. In contrast, the force–displacement response of the vertical isolation unit, which is acquired by superpositioning the force–



(b) Comparison of theoretical and experimental results

Fig. 7 Quasi-zero stiffness of the vertical isolation unit

displacement responses of the GAS structure and MNS dampers, performs a QZS characteristic in a very large displacement range from 6 to 34 mm. Furthermore, the stiffness of the vertical isolation unit is much closer to zero than both the GAS structure and MNS dampers, which means the vertical isolation unit can isolate the vibration better with lower transmissibility than GAS structure and MNS dampers. It is concluded from the above facts that a large QZS range with stiffness closer to zero can be obtained by combining nonlinear positive stiffness and nonlinear negative stiffness QZS components. The theoretical results of the vertical isolation unit is also compared with the experimental testing results in Fig. 7b, where they are matched in general.

3 Experimental characterisation of the quasi-zero stiffness and the tunable stiffness characteristics

After the manufacturing and assembling, the vertical lateral isolation units were tested to verify their QZS characteristic and tunable stiffness capability. The experiments are detailed in the following sections.

3.1 Experimental tests of the vertical isolation unit

3.1.1 Experimental setup

To characterise its mechanical property, the prototyped vertical isolation unit was tested by an MTS testing system (Load Frame Model: 370.02, MTS Systems Corp), as shown in Fig. 8. The unit was fixed between the upper and lower clamps of the system. Controlled by a computer and driven by a controller,

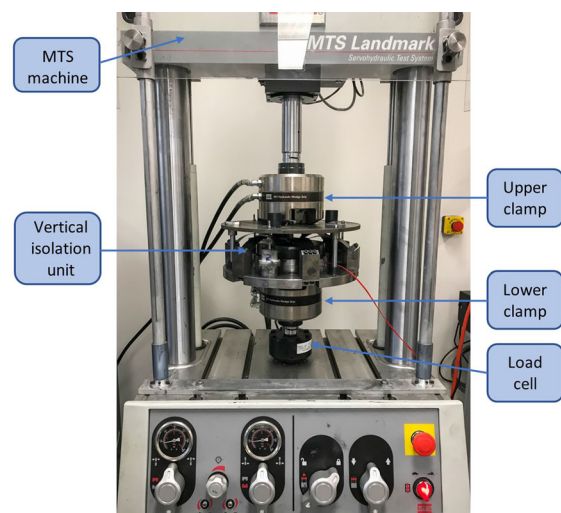


Fig. 8 Characterisation testing of the vertical isolation using an MTS testing system

the upper clamp moved vertically following the specific displacement commands. The lower clamp was fixed to the base of the MTS system via a load cell which can measure the real-time force. Meanwhile, the displacement of the upper clamp was also recorded by the system. A power supply was used to provide different levels of current to the coil of the vertical isolation unit.

3.1.2 The QZS characteristic test

To verify the QZS characteristic, the MRFs were not filled in the vertical isolation unit to avoid its influence on the stiffness. Firstly, the unit only installed with the GAS structure was tested to characterise the GAS structure. Then, MNS dampers were installed in addition to the GAS structure to acquire the superposition effect of them. The results of these tests under a harmonic displacement excitation with a frequency of 0.5 Hz are compared in Fig. 9. It is observed that the GAS structure performs a positive stiffness characteristic, and there is only 6 mm in the middle range performs QZS characteristics. With both the GAS structure and MNS dampers installed, the superpositioning stiffness of the vertical isolation unit is found to be 0.86 kN/m, which can be regarded as quasi-zero stiffness. This quasi-zero stiffness exists in a displacement range as large as 28 mm, almost 5 times of the GAS structure, indicating a large QZS range is realised by paralleling the GAS structure and MNS dampers.

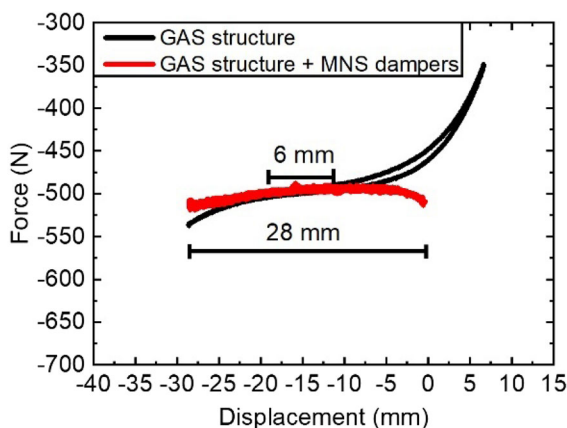


Fig. 9 Results of the QZS characteristic test

3.1.3 The tunable stiffness characteristic test

Following the quasi-zero stiffness characteristic test, the tunable stiffness characteristic of the vertical isolation unit with MRFs filled was experimentally evaluated. With the harmonic displacement excitation amplitude set as 0.25 mm, tests under three low frequencies, 0.1, 0.5 and 1.0 Hz, were conducted. In the tests, the coil of the vertical isolation unit was supplied with different current levels from 0 to 2.5 A with an increment of 0.5 A. The force–displacement responses under 0.1, 0.5 and 1 Hz with different applied currents are presented in Fig. 10. It is observed that the equivalent stiffness, represented by the ratio of force difference to displacement difference, increases obviously with the increase in the current under all frequency conditions. The reason for this phenomenon is that the viscosity of MRFs increases with the increase in the current, which hinders the relative motion between the top and base plates of the vertical isolation unit. The equivalent stiffness (calculated by referencing equation (2) in [11]) under different frequencies and currents is summarised in Table 1. Without current applied (0 A), the stiffness of the vertical isolation unit is very small, around 3.05 to 3.67 kN/mm, indicating the characteristic of quasi-zero stiffness is achieved. Under all frequency conditions, large stiffness variations by changing the current are observed. For instance, under the frequency condition of 1.0 Hz, the stiffness significantly increases from 3.67 to 81 kN/m when the current increases from 0 to 2.5 A. Additionally, with a fixed current, the vertical isolation unit performs a good consistency in stiffness under different frequency conditions, especially with currents 0, 1.0 and 1.5 A. The stiffness slightly varies when the current is 2.5 A. It is concluded from the above analysis that the large stiffness variation can be realised by changing the current, so the vertical isolation unit can adapt to different vibration excitations under various working conditions.

3.2 Experimental tests of the lateral isolation unit

3.2.1 Experimental setup

The prototyped lateral isolation unit was tested on a horizontal vibration platform, as shown in Fig. 11. The lateral isolation unit was mounted on the vibration

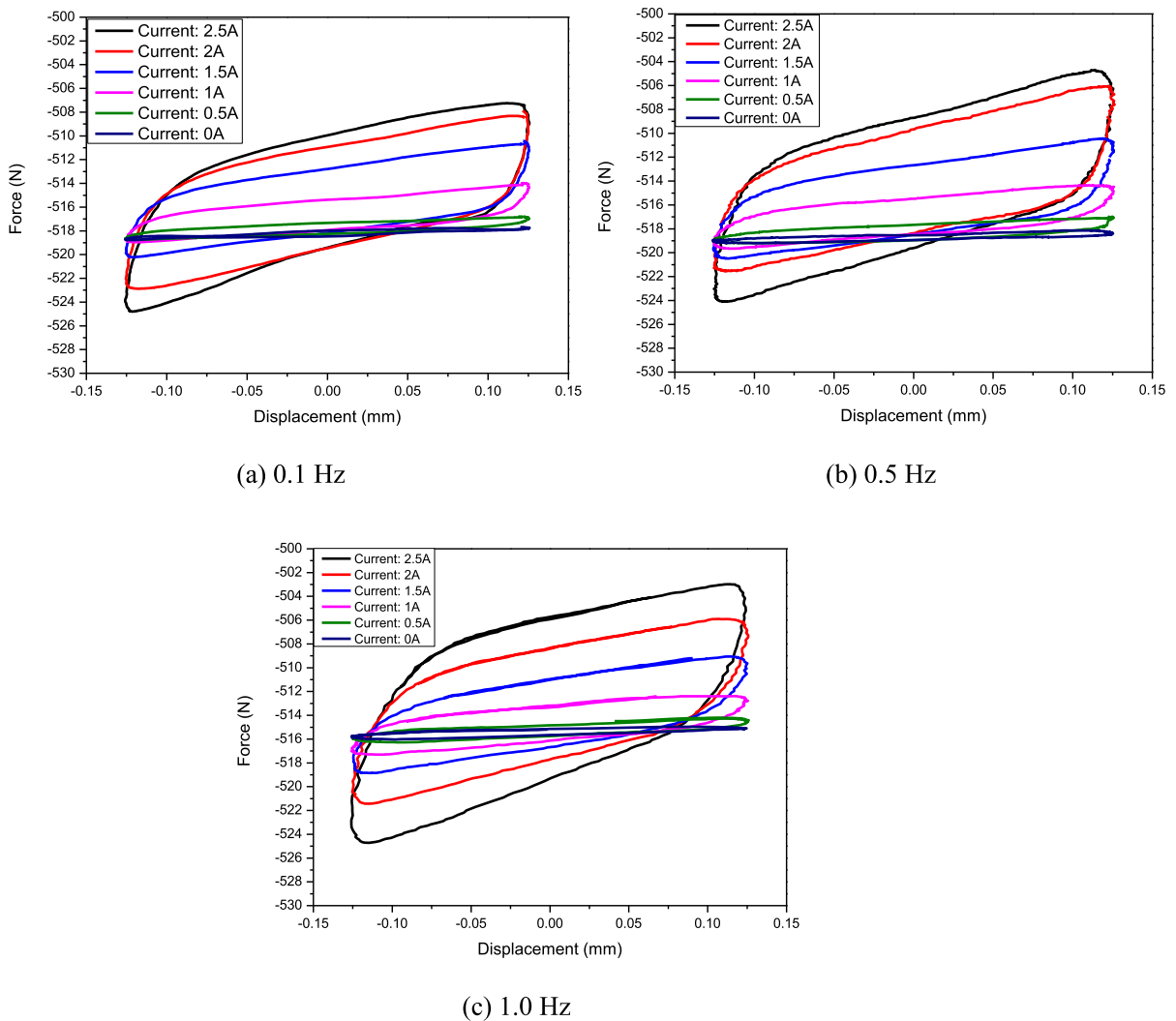


Fig. 10 Tunable stiffness characteristic of the vertical isolation unit via controlling the current

Table 1 Equivalent stiffness of the vertical isolation unit (kN/m)

Frequency (Hz)	Current					
	0 A (QZS)	0.5 A	1 A	1.5 A	2 A	2.5 A
0.1	3.05	7.28	18.8	37.56	57.16	69.48
0.5	3.29	7.48	20.16	38.8	61.12	76.88
1.0	3.67	7.32	18	38.2	56.48	81.08

plate, which is excited by an electrodynamic shaker (VTS, VC 100-8 vibration test system) and moves along with the sliding bearing. A laser displacement sensor (Micro-Epsilon, ILD1700-5) was used to measure the horizontal displacement of the isolation unit. A force sensor (Sinocera Piezotronics Inc. CA-

YD-302) was connected to a fixed pillar on one end and the isolated plate of the lateral isolation unit on the other, so it can measure the shear force of the plate given by the MRFs. A computer with a prepared LabVIEW program was manipulated to control the vibration excitation via a data acquisition board (NI,

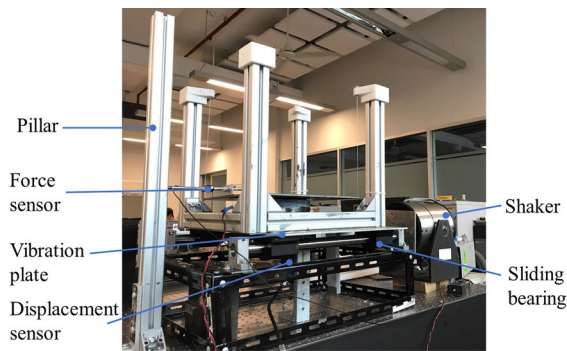


Fig. 11 Characterisation testing of the lateral isolation using a horizontal vibration platform

PCI-62). At the same time, the measured force and displacement data were collected via the data acquisition board and stored in the computer. A DC power supply (Thurlby Thandar Instruments Ltd) was also used to provide currents to the lateral isolation unit.

3.2.2 The QZS characteristic test

To verify the quasi-zero stiffness characteristic endowed by the pendulum structure, the influence of the MRFs should be avoided; hence, the tests were conducted without MRFs. Harmonic displacement signals with peak-to-peak displacements of 1, 2 and 3 mm and the frequency of 2, 5 and 10 Hz were selected as the excitations. The force–displacement responses at different frequencies are presented in Fig. 12 to investigate the effect of peak-to-peak displacement. The force–displacement responses at different peak-to-peak displacements are presented in Fig. 13 to investigate the effect of frequency.

It is seen from these two figures that the quasi-zero characteristic is realised as the stiffness of the force–displacement loop is very small and is close to zero under the different excitations. At the low vibration frequencies of 2 and 5 Hz (Fig. 12a, b), the force–displacement loops of small peak-to-peak displacements follow the trajectory of larger peak-to-peak displacements. Meanwhile, under small peak-to-peak displacements of 1 mm (Fig. 13a), the force–displacement responses show good repeatability with the increase in the frequency. It is also observed that, under conditions of large peak-to-peak displacements of 2 and 3 mm, and large frequencies of 10 Hz, the force–displacement responses behave a more obvious damping characteristic and the enclosed area of the

force–displacement becomes larger. This phenomenon is reasonable because the vibration velocity under these conditions is much larger than that of smaller displacements and lower frequencies, which induces the increase in the viscous force of MRFs.

3.2.3 The tunable stiffness characteristic test

After filling MRFs, the lateral isolation unit was tested to evaluate its tunable stiffness characteristics. During the tests, the frequency was fixed as 5 Hz, the peak-to-peak displacement was given as 0.1, 0.25 and 0.5 mm, and currents from 0 to 1.5 A with an increment of 0.5 A were provided. As shown in Fig. 14, under all the displacement conditions, the maximum force and the incline angle of the force–displacement loop increase following the increasing current, which is resulted from the increase in the MRFs' viscosity. The calculated equivalent stiffness is summarised in Table 2. It is seen that the lateral isolation unit can achieve quasi-zero stiffness characteristics with very small stiffness under all the displacement conditions when no current is applied (0 A). With the change of the current, a wide stiffness variation range is observed under all the peak-to-peak displacement conditions. For instance, the stiffness changes more than 81 times from 2 to 162.92 kN/m under the displacement condition of 0.5 mm when the current increases from 0 to 1.5 A.

4 Frequency response tests of the vertical and lateral isolation units

Transmissibility is an important index for a vibration isolation system that can reflect its performance. Hence, the vertical and lateral isolation units were separately tested to acquire the transmissibility of the proposed isolation system in the vertical and lateral directions. The experiments and the results of these isolation units are detailed in the following subsections.

4.1 The test and result analysis of the vertical isolation unit

The vertical isolation unit was tested by a six degree of freedom (six-DOF) vibration platform, as shown in Fig. 15. The electric cylinders of the platform were

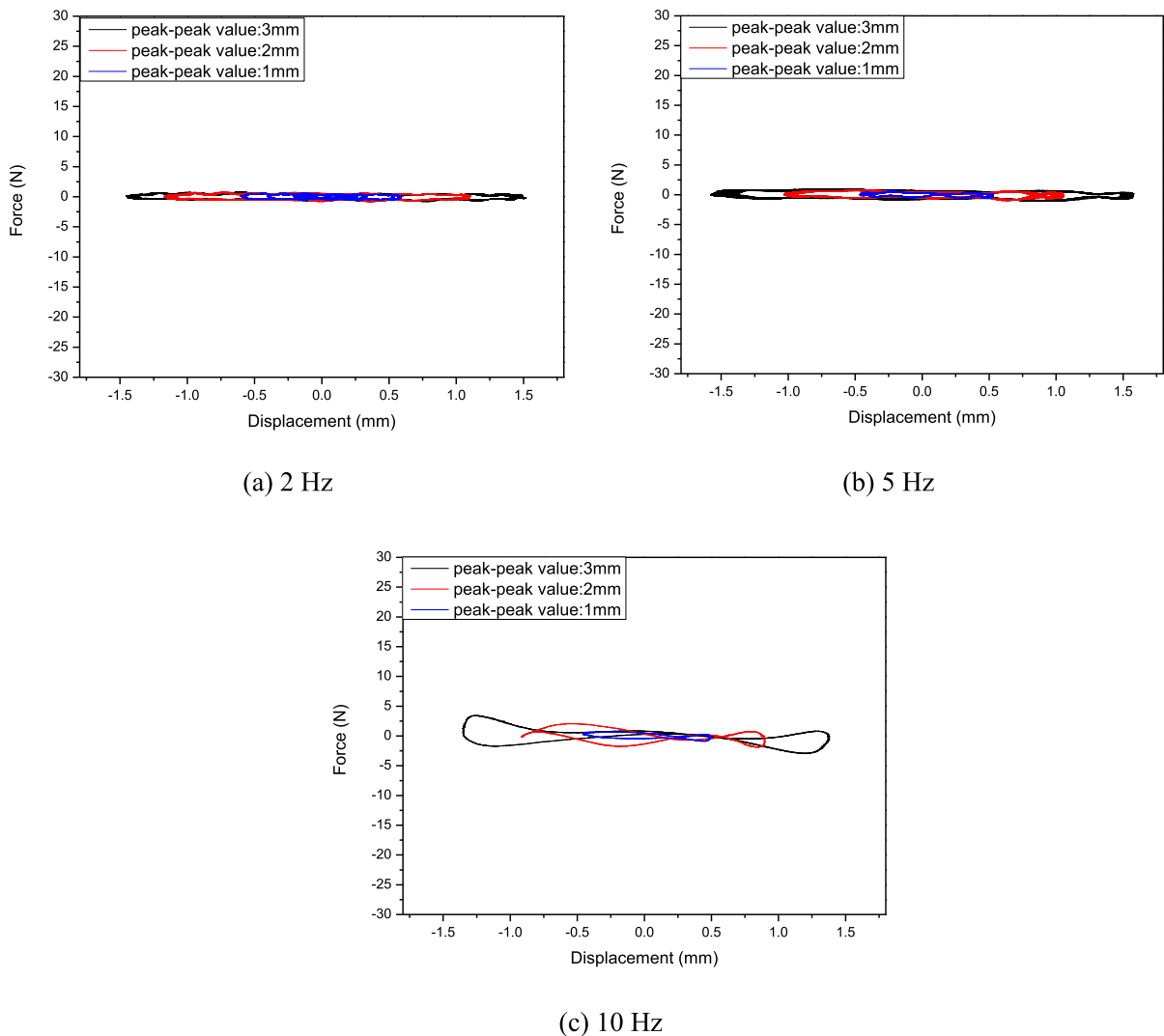


Fig. 12 QZS characteristics test results at different frequencies

driven by motor drives, which were controlled by computer 2 via an NI cRIO 9076. Hence, desired vertical excitations can be provided by this platform. The vertical isolation unit was mounted on the top plate of the platform, and a mass weighing 27 kg was loaded on it to make the initial displacement in the QZS range. Meanwhile, two acceleration sensors (Sinoceramics, Inc., CA-YD-113) were fixed to the plate of the vibration platform and the preloaded mass, respectively, to measure their vertical accelerations. The measured data were sent to computer 1 via an NI myRIO.

During the tests, a vertical vibration excitation with a sweeping frequency from 0 to 15 Hz was loaded to

the vertical isolation unit, and currents from 0 to 2 A with an increment of 0.5 A were applied. Transmissibility of the unit, defined as the acceleration ratio of the preloaded mass to the base of the isolation unit (or the top plate of the vibration platform), was acquired. It is noted that the lower the transmissibility, the less the vibration transmitted from the base to the preloaded mass, i.e. the better the vibration isolation performance. The result is presented in Fig. 16, and the corresponding data are summarised in Table 3. It is observed from the figure that the transmissibility curves are significantly affected by the change of current. Specifically, the resonance frequency, denoted by the peak of the transmissibility curve,

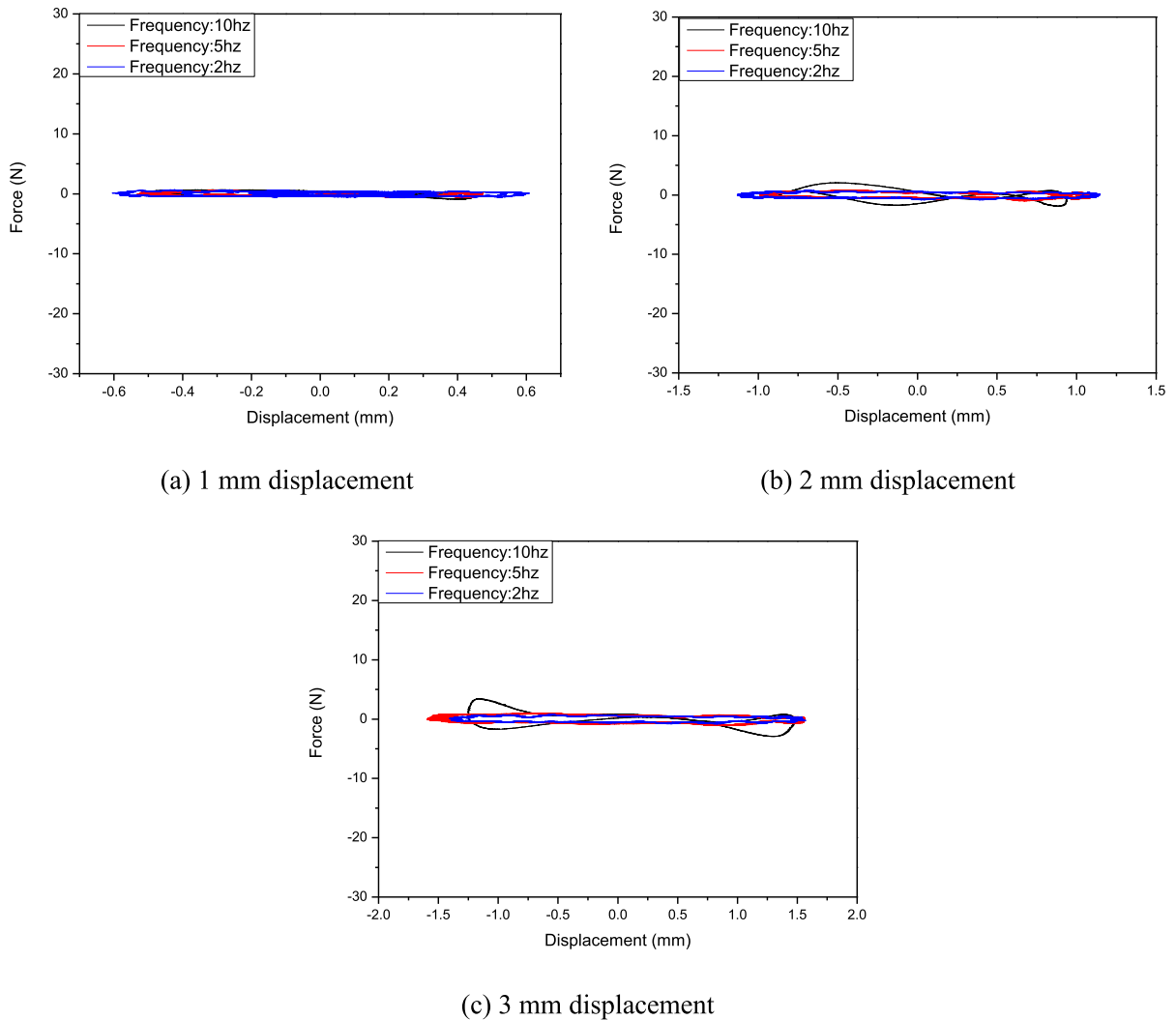


Fig. 13 QZS characteristics test results at different peak-to-peak displacements

rises 4.64 times from 1.4 to 6.5 Hz when the applied current increases from 0 to 2 A, whilst the maximum transmissibility decreases in general. This phenomenon occurred because a higher current resulted in high stiffness, which made the peak transmissibility shift to a higher frequency. The phenomenon indicated that the MRFs play an important role in changing the isolation performance of the vertical isolation unit by controlling the current. As shown in the figure, the largest stiffness (current: 2A) delivers the best isolation performance with the smallest transmissibility in the frequency range smaller than 2 Hz, and the smallest stiffness (current: 0A) performs best in the frequency range larger than 2 Hz. Hence, to achieve

the best vibration isolation performance in the vertical direction over the whole frequency range, the vertical vibration isolation control algorithm was designed as:

$$\begin{cases} f_z < 2 \text{ Hz}, & I_V = 2 \text{ A} \\ f_z \geq 2 \text{ Hz}, & I_V = 0 \text{ A} \end{cases} \quad (7)$$

where f_z and I_V are the excitation frequency and the current applied to the vertical isolation unit, respectively. With this control algorithm, the smallest transmissibility curve over the whole excitation frequency range can be realised, as shown by the controlled case in the figure.

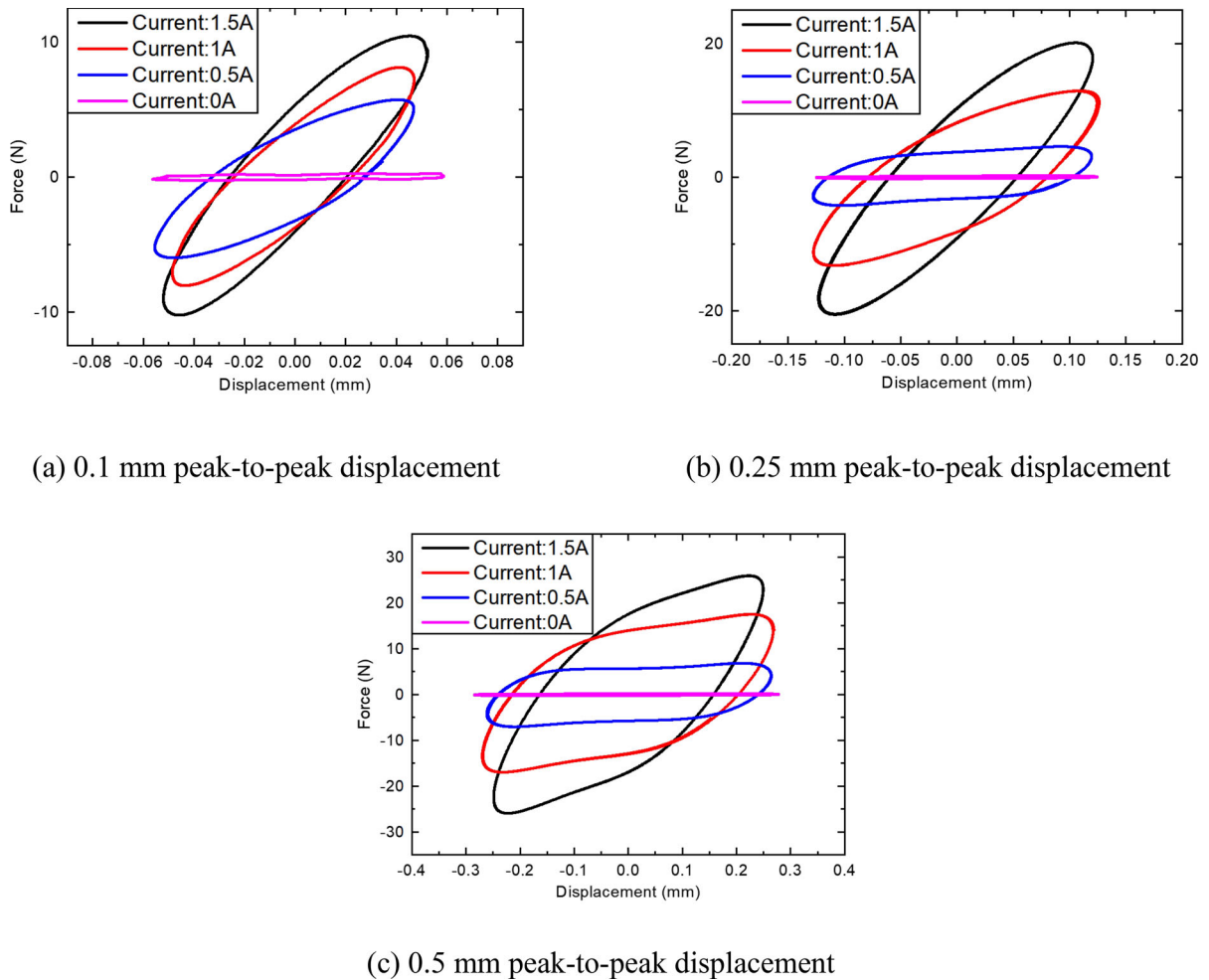


Fig. 14 Tunable stiffness characteristics of the lateral isolation unit via controlling the current

Table 2 Equivalent stiffness of the lateral isolation unit (kN/m)

Peak-to-peak displacement (mm)	Current			
	0 A (QZS)	0.5 A	1 A	1.5 A
0.1	4.8	116.1	160	207.5
0.25	2	35.6	103.72	162.92
0.5	2	35.6	103.72	162.92

4.2 The test and result analysis of the lateral isolation unit

As shown in Fig. 17, the lateral isolation unit was tested by the horizontal vibration platform introduced in Sect. 3.2.1. In the test, the vertical isolation unit and wooden frame were loaded on the lateral isolation unit. Two acceleration sensors (Sinoceramics, Inc.,

CA-YD-113) were fixed to the preloaded mass and the vibration platform, respectively. The measured accelerations of them were recorded for analysis. Lateral displacement excitation with a sweeping frequency from 0.2 to 15 Hz was applied to the system, and tests with different currents from 0 to 1.5 A with an increment of 0.5 A were implemented.

Fig. 15 Experimental setup of the vertical frequency response test

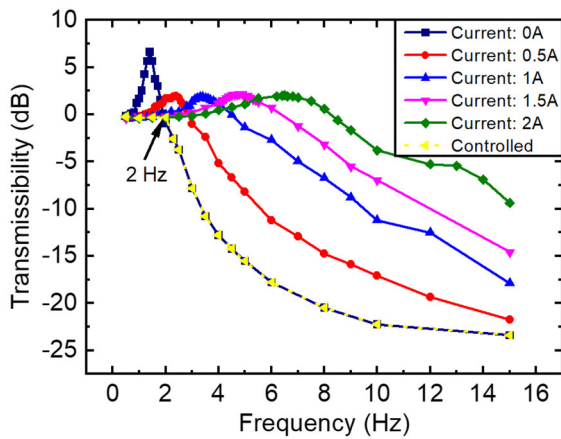
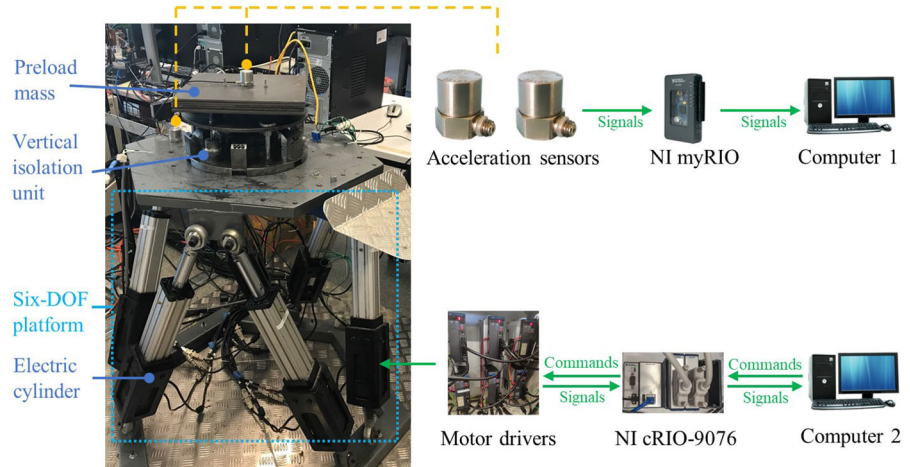


Fig. 16 Frequency response test results of the vertical isolation unit

The frequency response results are presented in Fig. 18, and the corresponding data are detailed in Table 4. It is seen that the transmissibility curve is largely affected by the applied current. When the current rises from 0 to 1.5 A, the resonant frequency increases 4.83 times from 0.95 to 4.59 Hz and the maximum transmissibility decreases from 20.12 to 4.57 dB. This phenomenon is similar to that of the vertical isolation unit. Because the largest stiffness

(current: 1.5 A) performs best in the low-frequency range smaller than 1.33 Hz and the smallest stiffness (current: 0 A) performs best in the high-frequency range larger than 1.33 Hz, the lateral vibration isolation control algorithm is designed as:

$$\begin{cases} f_x \text{ or } f_y < 1.33 \text{ Hz, } & I_L = 1.5 \text{ A} \\ \text{Else} & I_L = 0 \text{ A} \end{cases} \quad (8)$$

where f_x and f_y are the measured excitation frequencies in the lateral directions: x and y axes, and I_L is the current that applied to the lateral isolation unit. After utilising the above control algorithm, the controlled case in the figure delivered the best vibration isolation performance in the whole frequency range.

5 Experimental evaluation of the vibration isolation system

Following the transmissibility tests in the previous section, this section details the experimental evaluation of the vibration isolation system in terms of stability and vibration isolation performances.

Table 3 Resonance frequency and maximum transmissibility of the vertical isolation unit

Current (A)	0	0.5	1	1.5	2
Resonance frequency (Hz)	1.4	2.4	3.4	4.9	6.5
Maximum transmissibility (dB)	6.64	1.93	1.88	2.17	2.04

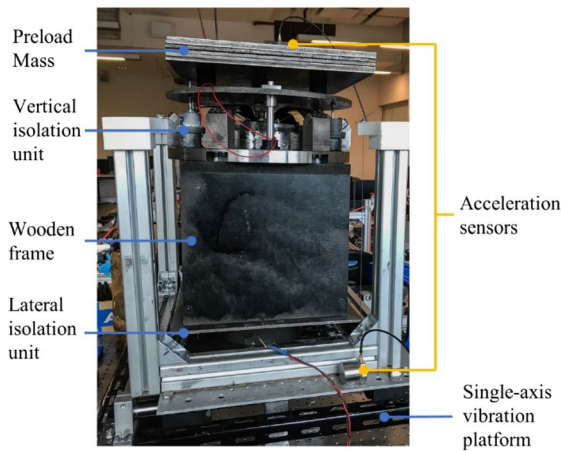


Fig. 17 Experimental setup of the lateral frequency response test

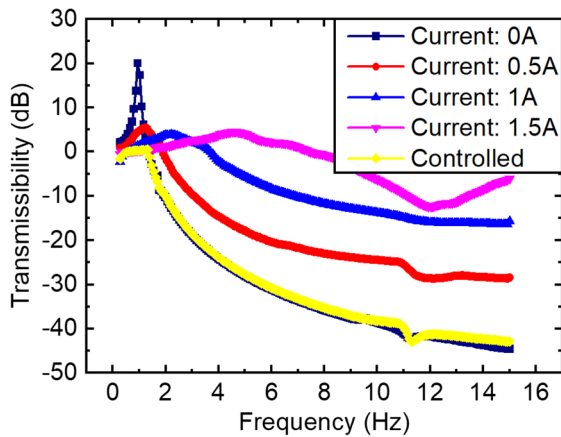


Fig. 18 Frequency responses test results of the lateral isolation unit

Table 4 Resonance frequency and maximum transmissibility of the lateral isolation unit

Current (A)	0	0.5	1	1.5
Resonant frequency (Hz)	0.95	1.24	2.14	4.59
Maximum transmissibility (dB)	20.12	5.38	3.79	4.57

5.1 Stability evaluation

In some applications, a system should remain highly stable during the operation process against external disturbances. For instance, the stability of the base-ment of a microscope should be ensured when

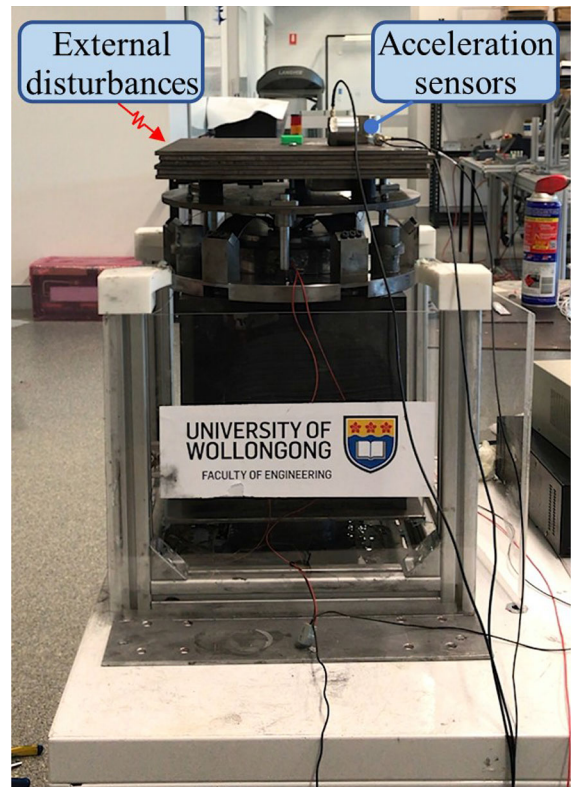


Fig. 19 Experimental setup for the stability evaluation test

changing the object slide; otherwise, extra calibration and adjustment will be required, which is undesirable and inefficient. The external disturbance is usually at an ultra-low frequency, and for the proposed isolation system, it is expected to act on the preloaded mass. A test shown in Fig. 19 was designed to evaluate the stability of the system. The external disturbance was simulated by pressing the mass with a hand. Then the data measured by the acceleration sensors (Sinoce-ramics, Inc., CA-YD-113) on the preloaded mass were sent to a computer for analysis. Hence, the stability against external disturbances of the system can be evaluated by the acceleration of the preloaded mass; the lower the acceleration, the better the stability. As follows, the computer sent the current command to amplifiers (YE5871A, Sinocera Piezotronics, Inc.) via an NI myRIO, so currents applied to the vertical and lateral vibration isolation units can be regulated.

The jerk, which is acquired by taking the derivative of the acceleration, was selected as the index to judge the magnitude of the external disturbance. Here, a jerk threshold value is set as 600 m/s^3 by experimental

experience to demonstrate the stability of the system; a disturbance with a jerk larger than the threshold is regarded as a large disturbance and vice versa. The control algorithm is designed as follows: if a large disturbance is detected, large currents will be given to the vertical and lateral isolation units to perform large stiffness so the system can sustain the external disturbance; otherwise, no current will be given, and the system remains the QZS state. Hence, the stability control algorithm is designed as:

$$\begin{aligned} & \text{IF } j_x \text{ or } j_y \geq 600 \text{ m/s}^3, I_L = 1.5\text{A} \\ & \text{Else } I_L = 0 \text{ A} \\ & \text{IF } j_z \geq 600 \text{ m/s}^3, I_V = 2 \text{ A} \\ & \text{Else } I_V = 0 \text{ A} \end{aligned} \quad (9)$$

where j_x , j_y and j_z are the jerk values in the x , y and z directions, respectively, and they are derived by differentiating the real-time acceleration data.

As the vibration isolation system can vary the stiffness both laterally and vertically, a downward press with 45° was acted on the preloaded mass in the yz -plane to simultaneously evaluate the stability of the system in the lateral and vertical directions. Both the test with the pure QZS (0 A) and the test with the designed stability control algorithm (Eq. (9)) were conducted, and the results are presented in Fig. 20. It is seen that, when no current is applied and the system is in the pure QZS state (red data), the preloaded mass suffers large fluctuations in x , y and z axials. In contrast, the fluctuations are significantly reduced in the controlled case (black data) via regulating the stiffness of the system (also see Video 1). This is because large stiffness was applied when the isolation system suffered external disturbances, so the preloaded mass has less vibration in the controlled case. Based on the analysis, it is concluded that the system with pure QZS characteristics is unstable from external disturbances such as impact and low-frequency vibration, and the stability of the system is largely improved by adding the variable stiffness feature with MRFs components.

5.2 Vibration isolation evaluation

Following the stability testing, the proposed isolation system was evaluated by the six-DOF vibration platform with random vibration excitations. As shown in the experimental setup in Fig. 21, the vibration

isolation system is fixed to the six-DOF vibration platform. Sensors ($3 \times$ CA-YD-113 Sinoceramics, Inc. and $3 \times$ ADXL203EB, Analog Devices, Inc.) were mounted on the platform and the preloaded mass, respectively, to measure the accelerations of them in x , y and z axes, and the measured data were sent back to Computer 1 via an NI myRIO. Through analysing the real-time acceleration data, the dominant frequency of the vibration excitation can be determined in real time by the short-time Fourier transform (STFT) module in the LabVIEW programme. Then, commands of Computer 1 were sent to amplifiers (YE5871A, Sinocera Piezotronics, Inc.) so that the currents applied to the vertical and lateral isolation units were controlled based on the vibration isolation control algorithms (Eqs. (7) and (8)). Additionally, two beakers with red liquid are mounted on the vibration platform and the preloaded mass, respectively, to demonstrate their vibration levels in the recorded videos of the attached supplement.

In order to test the vibration isolation performance, a random vibration signal, which is composed of a range of random frequencies and magnitudes in x , y and z axes, was selected to act as excitation. Tests of QZS ($I_L = I_V = 0 \text{ A}$), large stiffness ($I_L = 1.5 \text{ A}, I_V = 2 \text{ A}$) and QZS with the vibration isolation control algorithm were conducted.

Firstly, the vibration isolation performance of the QZS characteristic was evaluated by applying no currents to the vertical and lateral vibration units ($I_L = I_V = 0 \text{ A}$). The test result is presented in Fig. 22, in which Fig. 22a and b show the accelerations in the time domain of the platform (excitation) and the preloaded mass (response), respectively. It is seen that the acceleration amplitudes of the platform (excitation) in x , y and z axes are around $4\text{--}8 \text{ m/s}^2$, whilst the acceleration amplitudes of the preloaded mass (response) are around $0.003\text{--}0.03 \text{ m/s}^2$, which is much smaller than the platform. The result indicates that the QZS characteristic of the proposed isolation system can significantly isolate the vibration transferred from the platform to the preloaded mass in both the vertical and lateral directions.

Then, the vibration isolation performances of large stiffness ($I_L = 1.5 \text{ A}, I_V = 2 \text{ A}$), QZS ($I_L = I_V = 0 \text{ A}$) and QZS with the vibration isolation control algorithm were compared by analysing their preloaded mass acceleration in x , y and z axes, as shown in Fig. 23. It is seen that the QZS case and

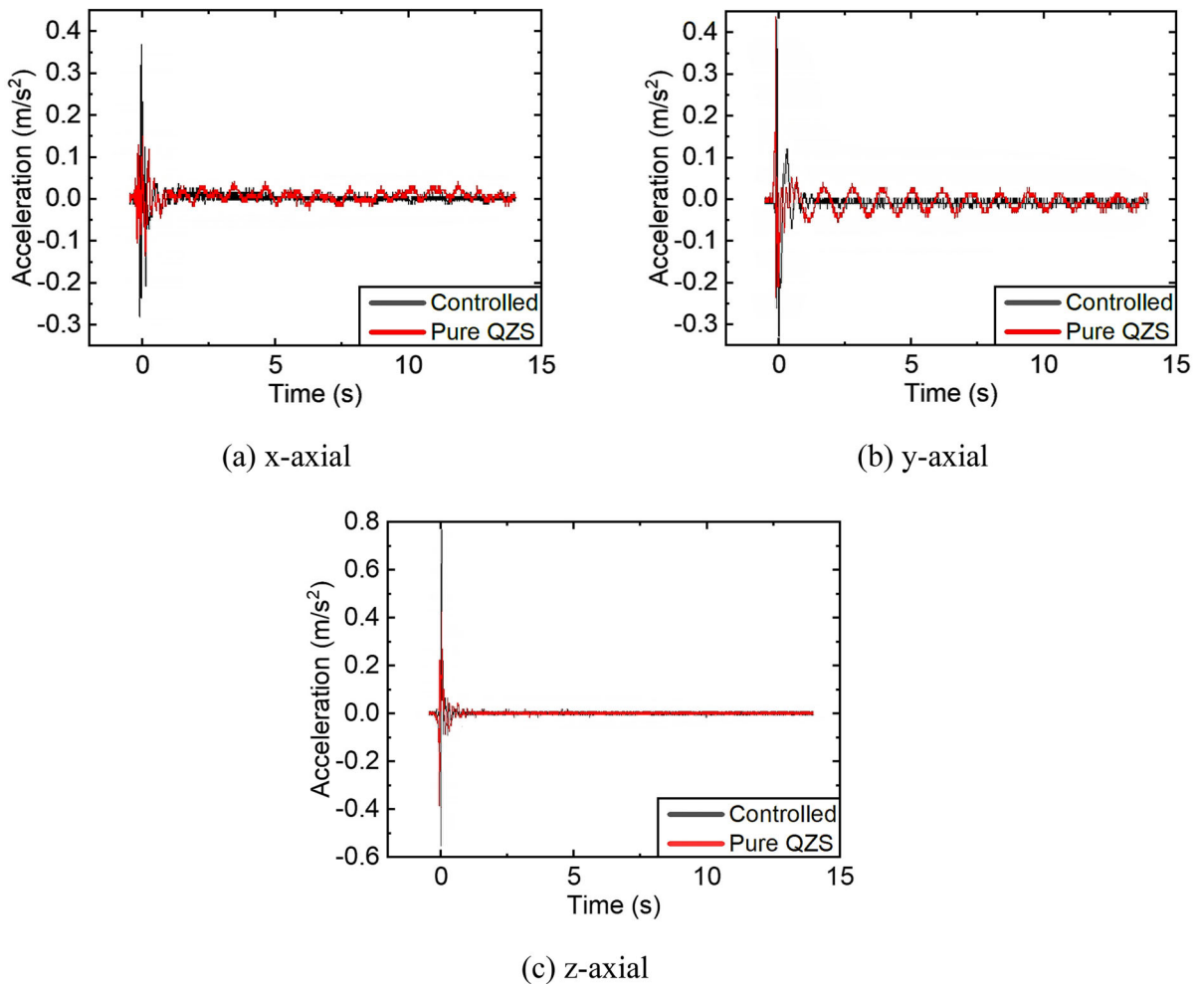
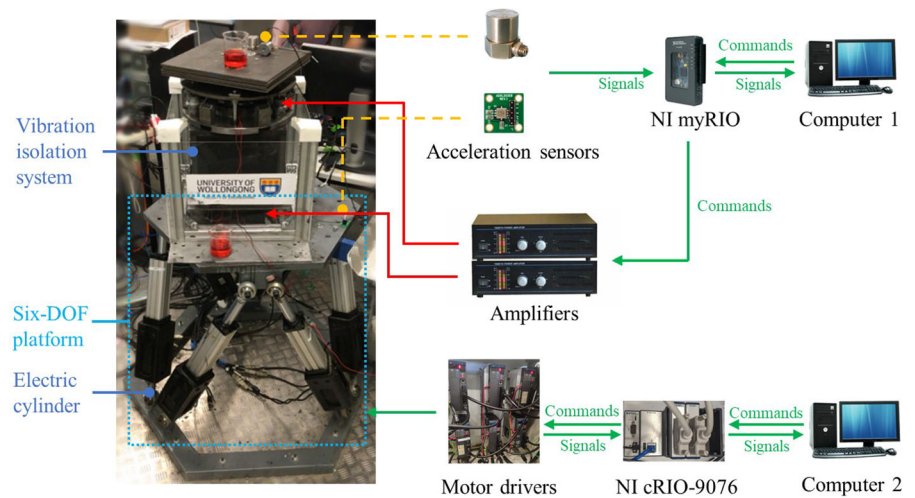


Fig. 20 Results of the stability evaluation test

Fig. 21 Experimental setup of the vibration evaluation test



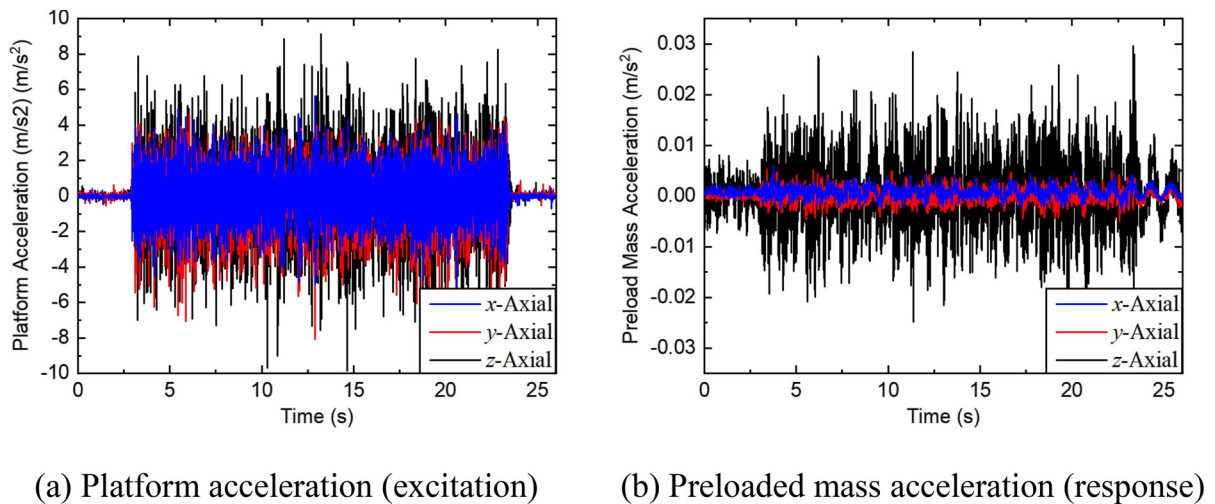


Fig. 22 Test result of the vibration isolation system with QZS characteristics ($I_L = I_V = 0$ A)

controlled QZS case have much smaller acceleration amplitudes than the large stiffness case in all axes, which verifies the effectiveness of the QZS characteristic in vibration isolation. The controlled QZS case delivers better vibration isolation performance than the QZS case via regulating the current/stiffness of the system. In the recorded video (Video 2), the vibration of the preloaded mass (demonstrated by the shaking of the red liquid) of the controlled QZS case is significantly smaller than that of the large stiffness case.

The root mean square (RMS) value of the preloaded mass acceleration is summarised in Table 5 for further analysis. It is found that in all axes, the controlled QZS has the smallest RMS value among all cases, which means the preloaded mass has the smallest vibration under the controlled QZS case. Compared with the QZS case, the RMS values of the controlled QZS case reduced 26.8%, 11.8% and 5.2% in x , y and z axes, respectively, denoting the vibration isolation performance of the QZS characteristics can be further improved by controlling the stiffness of the system.

Based on the analysis of the stability evaluation and vibration isolation evaluation tests, it is concluded that the proposed vibration isolation system with QZS and tunable stiffness characteristics is capable of realising excellent vibration isolation performance with high stability against external disturbances.

6 Conclusion

In this paper, a highly stable QZS vibration isolation system with a large QZS range is designed, prototyped and experimentally evaluated. Consisting of vertical and lateral vibration isolation units featuring QZS, the system can simultaneously isolate vibration both vertically and laterally. Meanwhile, their tunable stiffness characteristics can keep the system stable against external disturbances, which overcomes the inherently unstable feature of existing QZS systems. Additionally, the QZS range of the vertical vibration isolation unit is enlarged by paralleling nonlinear negative and positive QZS components; hence, it can deliver QZS characteristics in a larger displacement range. Control algorithms for vibration isolation and stability were designed, and testing platforms were established. The QZS and the tunable stiffness characteristics of the vertical and lateral vibration isolation units have been experimentally validated; the stability and the vibration isolation performance of the prototyped system have been evaluated. The main contributions are concluded as follows:

- (1) By paralleling the nonlinear positive QZS component, the GAS structure, with the nonlinear negative QZS component, the MNS dampers, the vertical isolation unit has a QZS range of 28 mm, which is larger than that of the GAS structure by 18 mm. Meanwhile, the stiffness is

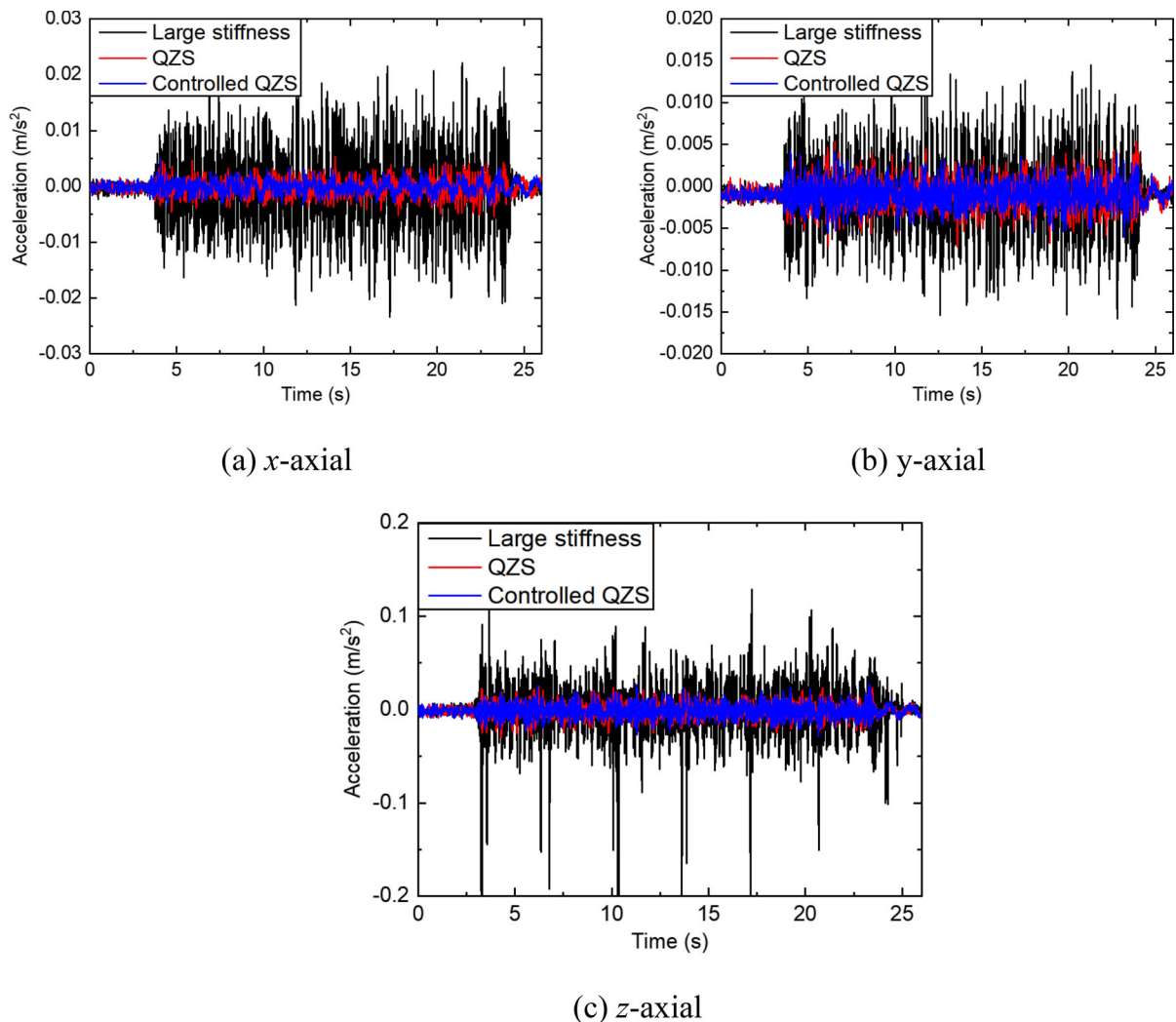


Fig. 23 Preloaded mass acceleration in different cases

Table 5 Root mean square (RMS) values of the preloaded mass acceleration

	Large stiffness	QZS	Controlled QZS
<i>x</i> axis	0.00724	0.00164	0.00120
<i>y</i> axis	0.00500	0.00202	0.00178
<i>z</i> axis	0.03426	0.00820	0.00777

also decreased by paralleling these two components so the system can deliver better vibration isolation performance.

- (2) The tunable stiffness of the vibration isolation system is verified experimentally. The stiffness

of the vertical isolation unit changes from 3.05 to 69.48 kN/m when the current increases from 0 to 2.5 A, and the stiffness of the lateral isolation unit changes from 4.8 to 207.5 kN/m when the current increases from 0 to 1.5 A.

- (3) The transmissibility curves of the vertical and lateral isolation units are significantly affected by the tunable stiffness. The lowest transmissibility curve in the whole frequency range is achieved by setting large stiffness in the low-frequency range and small stiffness in the high-frequency range. With the designed vibration isolation control algorithms, the best vibration isolation performance indicated by the lowest

transmissibility in the whole frequency range can be realised.

- (4) The experimental test verified that the stability of the vibration isolation system is significantly improved by controlling the stiffness according to the designed stability algorithm when the system suffers external disturbances. In this way, the unstable problem of the conventional QZS system is solved.
- (5) The vibration isolation performance of the proposed system is experimentally evaluated. The results show that both the vertical and lateral vibrations can be isolated by the QZS characteristic to a large extent. Additionally, via regulating the stiffness of the system based on the control algorithms, the isolation performance is further improved.

Future work may focus on designing a more compact magnetorheological isolation system with a simpler structure to reduce manufacturing difficulties and expenses.

Funding Open Access funding enabled and organized by CAUL and its Member Institutions. This research is supported by the Australian Research Council Linkage Grants (Nos. LP190100603 and LP210301054) and the Australian Research Council Discovery Grant (DP200100149).

Data availability Data sharing not applicable to this article as no datasets were generated or analysed during the current study.

Declarations

Conflict of interest The authors declare that they have no conflicts of interest.

Open Access This article is licensed under a Creative Commons Attribution 4.0 International License, which permits use, sharing, adaptation, distribution and reproduction in any medium or format, as long as you give appropriate credit to the original author(s) and the source, provide a link to the Creative Commons licence, and indicate if changes were made. The images or other third party material in this article are included in the article's Creative Commons licence, unless indicated otherwise in a credit line to the material. If material is not included in the article's Creative Commons licence and your intended use is not permitted by statutory regulation or exceeds the permitted use, you will need to obtain permission directly from the copyright holder. To view a copy of this licence, visit <http://creativecommons.org/licenses/by/4.0/>.

References

1. Blood, R.P., Yost, M.G., Camp, J.E., Ching, R.P.: Whole-body vibration exposure intervention among professional bus and truck drivers: a laboratory evaluation of seat-suspension designs. *J. Occup. Environ. Hyg.* **12**, 351–362 (2015)
2. Burdorf, A., Swuste, P.: The effect of seat suspension on exposure to whole-body vibration of professional drivers. *Ann. Occup. Hyg.* **37**, 45–55 (1993)
3. Yu, Y., Royel, S., Li, Y., Li, J., Yousefi, A.M., Gu, X., Li, S., Li, H.: Dynamic modelling and control of shear-mode rotational MR damper for mitigating hazard vibration of building structures. *Smart Mater. Struct.* **29**, 114006 (2020)
4. Deng, L., Sun, S., Christie, M., Ning, D., Jin, S., Du, H., Zhang, S., Li, W.: Investigation of a seat suspension installed with compact variable stiffness and damping rotary magnetorheological dampers. *Mech. Syst. Signal Process.* **171**, 108802 (2022)
5. Yoon, D.-S., Kim, G.-W., Choi, S.-B.: Response time of magnetorheological dampers to current inputs in a semi-active suspension system: modeling, control and sensitivity analysis. *Mech. Syst. Signal Process.* **146**, 106999 (2021)
6. Oh, J.-S., Jeon, K., Kim, G.-W., Choi, S.-B.: Dynamic analysis of semi-active MR suspension system considering response time and damping force curve. *J. Intell. Mater. Syst. Struct.* **32**, 1462–1472 (2021)
7. Boluhari, S.M., Masih-Tehrani, M., Yahyaei, R., Marzbanrad, J.: Seat-driver vibration parameters effect on horizontal driver acceleration and its relationship to driver mass. *Int. J. Hydromechatron.* **3**, 281–296 (2020)
8. Zha, J., Nguyen, V., Su, B., Jiao, R., Ni, D.: Performance of the seat suspension system using negative stiffness structure on improving the driver's ride comfort. *SAE Int. J. Veh. Dyn. Stab. NVH* **6**, 135–146 (2022)
9. Kwon, H., Song, Y., Park, J.-E., Kim, Y.-K.: A standalone tunable vibration absorber with self-sensing magnetorheological elastomer. *Smart Mater. Struct.* **30**, 115010 (2021)
10. Yuan, L., Sun, S., Pan, Z., Ding, D., Gienke, O., Li, W.: Mode coupling chatter suppression for robotic machining using semi-active magnetorheological elastomers absorber. *Mech. Syst. Signal Process.* **117**, 221–237 (2019)
11. Deng, L., Sun, S., Christie, M.D., Yang, J., Ning, D., Zhu, X., Du, H., Zhang, S., Li, W.: Experimental testing and modelling of a rotary variable stiffness and damping shock absorber using magnetorheological technology. *J. Intell. Mater. Syst. Struct.* **30**, 1453–1465 (2019)
12. Li, H., Li, Y., Li, J.: Negative stiffness devices for vibration isolation applications: a review. *Adv. Struct. Eng.* **23**, 1739–1755 (2020)
13. Gu, X., Li, J., Li, Y.: Experimental realisation of the real-time controlled smart magnetorheological elastomer seismic isolation system with shake table. *Struct. Control. Health Monit.* **27**, e2476 (2020)
14. Li, Y., Li, J.: Overview of the development of smart base isolation system featuring magnetorheological elastomer. *Smart Struct. Syst.* **24**, 37–52 (2019)
15. Yu, J., Dong, X., Qi, S., Wang, T., Liang, Y.: Development of a magnetorheological isolator with variable damping and

- variable stiffness for broadband vibration suppression. *Smart Mater. Struct.* **30**, 025023 (2021)
16. Chen, Z., Sun, S., Deng, L., Yang, J., Zhang, S., Du, H., Li, W.: Investigation of a new metamaterial magnetorheological elastomer isolator with tunable vibration bandgaps. *Mech. Syst. Signal Process.* **170**, 108806 (2022)
 17. Crede, C.E., Ruzicka, J.E.: Theory of vibration isolation. *Shock Vib. Handb.* **2**, 30–35 (1996)
 18. Jin, S., Sun, S., Yang, J., Deng, L., Du, H., Li, W.: A hybrid MRE isolation system integrated with ball-screw inerter for vibration control. *Smart Mater. Struct.* **31**, 025009 (2021)
 19. Yang, J., Sun, S., Tian, T., Li, W., Du, H., Alici, G., Nakano, M.: Development of a novel multi-layer MRE isolator for suppression of building vibrations under seismic events. *Mech. Syst. Signal Process.* **70**, 811–820 (2016)
 20. Yu, Y., Royel, S., Li, J., Li, Y., Ha, Q.: Magnetorheological elastomer base isolator for earthquake response mitigation on building structures: modeling and second-order sliding mode control. *Earthq. Struct.* **11**, 943–966 (2016)
 21. Yang, J., Christie, M., Sun, S., Ning, D., Nakano, M., Li, Z., Du, H., Li, W.: Integration of an omnidirectional self-powering component to an MRE isolator towards a smart passive isolation system. *Mech. Syst. Signal Process.* **144**, 106853 (2020)
 22. Zeng, R., Yin, S., Wen, G., Zhou, J.: A non-smooth quasi-zero-stiffness isolator with displacement constraints. *Int. J. Mech. Sci.* **225**, 107351 (2022)
 23. Zuo, S., Wang, D., Zhang, Y., Luo, Q.: Design and testing of a parabolic cam-roller quasi-zero-stiffness vibration isolator. *Int. J. Mech. Sci.* **220**, 107146 (2022)
 24. Shaw, A., Gatti, G., Gonçalves, P., Tang, B., Brennan, M.: Design and test of an adjustable quasi-zero stiffness device and its use to suspend masses on a multi-modal structure. *Mech. Syst. Signal Process.* **152**, 107354 (2021)
 25. Ye, K., Ji, J., Brown, T.: Design of a quasi-zero stiffness isolation system for supporting different loads. *J. Sound Vib.* **471**, 115198 (2020)
 26. Liu, S., Feng, L., Zhao, D., Shi, X., Zhang, Y., Jiang, J., Zhao, Y., Zhang, C., Chen, L.: A real-time controllable electromagnetic vibration isolator based on magnetorheological elastomer with quasi-zero stiffness characteristic. *Smart Mater. Struct.* **28**, 085037 (2019)
 27. Sadeghi, S., Li, S.: Fluidic origami cellular structure with asymmetric quasi-zero stiffness for low-frequency vibration isolation. *Smart Mater. Struct.* **28**, 065006 (2019)
 28. Ding, H., Ji, J., Chen, L.-Q.: Nonlinear vibration isolation for fluid-conveying pipes using quasi-zero stiffness characteristics. *Mech. Syst. Signal Process.* **121**, 675–688 (2019)
 29. Li, M., Cheng, W., Xie, R.: A quasi-zero-stiffness vibration isolator using a cam mechanism with user-defined profile. *Int. J. Mech. Sci.* **189**, 105938 (2021)
 30. Alabuzhev, P.: *Vibration Protection and Measuring Systems with Quasi-zero Stiffness*. CRC Press, Boca Raton (1989)
 31. Carrella, A., Brennan, M., Waters, T.: Static analysis of a passive vibration isolator with quasi-zero-stiffness characteristic. *J. Sound Vib.* **301**, 678–689 (2007)
 32. Kovacic, I., Brennan, M.J., Waters, T.P.: A study of a nonlinear vibration isolator with a quasi-zero stiffness characteristic. *J. Sound Vib.* **315**, 700–711 (2008)
 33. Lan, C.-C., Yang, S.-A., Wu, Y.-S.: Design and experiment of a compact quasi-zero-stiffness isolator capable of a wide range of loads. *J. Sound Vib.* **333**, 4843–4858 (2014)
 34. Zhao, F., Ji, J., Ye, K., Luo, Q.: Increase of quasi-zero stiffness region using two pairs of oblique springs. *Mech. Syst. Signal Process.* **144**, 106975 (2020)
 35. Duan, Y., Wei, X., Wang, H., Zhao, M., Ren, Z., Zhao, H., Ren, J.: Design and numerical performance analysis of a microgravity accelerometer with quasi-zero stiffness. *Smart Mater. Struct.* **29**, 075018 (2020)
 36. Cai, C., Zhou, J., Wang, K., Pan, H., Tan, D., Xu, D., Wen, G.: Flexural wave attenuation by metamaterial beam with compliant quasi-zero-stiffness resonators. *Mech. Syst. Signal Process.* **174**, 109119 (2022)
 37. Xiong, Y., Li, F., Wang, Y.: A nonlinear quasi-zero-stiffness vibration isolation system with additional X-shaped structure: theory and experiment. *Mech. Syst. Signal Process.* **177**, 109208 (2022)
 38. Hu, X., Zhou, C.: The effect of various damping on the isolation performance of quasi-zero-stiffness system. *Mech. Syst. Signal Process.* **171**, 108944 (2022)
 39. Gatti, G., Shaw, A., Gonçalves, P., Brennan, M.: On the detailed design of a quasi-zero stiffness device to assist in the realisation of a translational Lanchester damper. *Mech. Syst. Signal Process.* **164**, 108258 (2022)
 40. Lin, Q., Zhou, J., Wang, K., Xu, D., Wen, G., Wang, Q., Cai, C.: Low-frequency locally resonant band gap of the two-dimensional quasi-zero-stiffness metamaterials. *Int. J. Mech. Sci.* **222**, 107230 (2022)
 41. Chang, Y., Zhou, J., Wang, K., Xu, D.: Theoretical and experimental investigations on semi-active quasi-zero-stiffness dynamic vibration absorber. *Int. J. Mech. Sci.* **214**, 106892 (2022)
 42. Wen, G., He, J., Liu, J., Lin, Y.: Design, analysis and semi-active control of a quasi-zero stiffness vibration isolation system with six oblique springs. *Nonlinear Dyn.* **106**, 309–321 (2021)
 43. Chen, T., Zheng, Y., Song, L., Gao, X., Li, Z.: Design of a new quasi-zero-stiffness isolator system with nonlinear positive stiffness configuration and its novel features. *Nonlinear Dyn.* **111**, 5141–5163 (2023)
 44. Cheng, C., Hu, Y., Ma, R., Wang, W.: Beneficial performance of a quasi-zero-stiffness vibration isolator with displacement-velocity feedback control. *Nonlinear Dyn.* **111**, 5165–5177 (2023)
 45. Chai, Y., Jing, X.: Low-frequency multi-direction vibration isolation via a new arrangement of the X-shaped linkage mechanism. *Nonlinear Dyn.* **109**, 2383–2421 (2022)
 46. An, J., Chen, G., Deng, X., Xi, C., Wang, T., He, H.: Analytical study of a pneumatic quasi-zero-stiffness isolator with mistuned mass. *Nonlinear Dyn.* **108**, 3297–3312 (2022)
 47. Zhou, J., Wang, X., Xu, D., Bishop, S.: Nonlinear dynamic characteristics of a quasi-zero stiffness vibration isolator with cam-roller-spring mechanisms. *J. Sound Vib.* **346**, 53–69 (2015)
 48. Liu, X., Huang, X., Hua, H.: On the characteristics of a quasi-zero stiffness isolator using Euler buckled beam as negative stiffness corrector. *J. Sound Vib.* **332**, 3359–3376 (2013)

49. Shaw, A., Neild, S., Wagg, D., Weaver, P., Carrella, A.: A nonlinear spring mechanism incorporating a bistable composite plate for vibration isolation. *J. Sound Vib.* **332**, 6265–6275 (2013)
50. De Vicente, J., Klingenberg, D.J., Hidalgo-Alvarez, R.: Magnetorheological fluids: a review. *Soft Matter* **7**, 3701–3710 (2011)
51. Ahamed, R., Choi, S.-B., Ferdous, M.M.: A state of art on magneto-rheological materials and their potential applications. *J. Intell. Mater. Syst. Struct.* **29**, 2051–2095 (2018)
52. Zhu, X., Jing, X., Cheng, L.: Magnetorheological fluid dampers: a review on structure design and analysis. *J. Intell. Mater. Syst. Struct.* **23**, 839–873 (2012)
53. Yan, L., Xuan, S., Gong, X.: Shock isolation performance of a geometric anti-spring isolator. *J. Sound Vib.* **413**, 120–143 (2018)
54. Yan, L., Gong, X.: Experimental study of vibration isolation characteristics of a geometric anti-spring isolator. *Appl. Sci.* **7**, 711 (2017)
55. Shi, X., Zhu, S.: Simulation and optimization of magnetic negative stiffness dampers. *Sens. Actuators A* **259**, 14–33 (2017)
56. Coey, J.: Permanent magnet applications. *J. Magn. Magn. Mater.* **248**, 441–456 (2002)

Publisher's Note Springer Nature remains neutral with regard to jurisdictional claims in published maps and institutional affiliations.